IAA-BR-07-01

Attitude Control Model for CubeSats

Molina, Juan Carlos, Ayerdi, Víctor**, Zea, Luis****

An essential step in the attitude control system design process is the construction of a simulation model that is sufficiently accurate to represent system dynamics, thus allowing for algorithm validation and performance testing. There aren't many publications or models that serve as a basis for designing and understanding a satellite's attitude determination and control system from a CubeSat's standpoint. Faced with this challenge, an attitude control model was designed and evaluated for its use on a CubeSat. The model is intended for CubeSats with an active control scheme based on reaction wheels. A model that combines a CubeSat's transfer function with the attitude control algorithm was developed in order to simulate closed-loop system response. The operational requirements and scientific drivers of Guatemala's first CubeSat mission, remote sensing for lake contamination monitoring, were utilized as input parameters for the simulation model. An additional simulation was performed in order to characterize the environmental disturbances that the control system must be able to reject. The simulation model for continuous attitude control was translated to an equivalent discrete model that enables the results to be implemented in a real-time embedded system. The simulation model was used to determine adequate Proportional-Integral-Derivative controller gains.

Keywords - Attitude Control, CubeSat Plant, Disturbance Torques, Reaction Wheel, Multi-loop controller, Emulation.

I. Introduction

A satellite's attitude refers to the spacecraft's position and orientation with respect to an object, e.g. Earth, and its control is of paramount importance to orient instruments (e.g. antennae or remote sensing devices) in the right direc-

* Universidad del Valle de Guatemala, Guatemala, email: jcmolina@uvg.edu.gt
** Universidad del Valle de Guatemala, Guatemala, email: vhayerdi@uvg.edu.gt
*** Universidad del Valle de Guatemala, Guatemala, email: lpzea@uvg.edu.gt

tion. As a satellite orbits Earth, disturbance torques are applied on it by atmospheric, magnetic, and gravitational conditions. Through the use of feedback loops, an Attitude Determination and Control Subsystem (ADCS) is capable of stabilizing and orienting a satellite by rejecting the external disturbances present in the orbital environment. While an ADCS manages attitude determination and control, this work focuses on attitude control.

The instantaneous attitude of a satellite can be described using angle measurements with respect to an inertial frame of reference. This frame uses the velocity vector as the +x axis, the direction of the local zenith as the +z axis, and the +y axis is chosen to be perpendicular to the orbital plane in order to comply with the right hand rule. A second frame of reference, known as the satellite frame, is defined using the satellites principal axes of inertia. The satellite frame moves together with the satellite's structure when the attitude changes. The angles necessary to rotate the inertial frame so that it coincides with the satellite's body frame are known as the Euler angles. Rotating about the x-, y-, and z-axis is known as a roll, pitch, and yaw rotations, respectively. In this paper, the rotation angles are indicated as φ, θ, and ψ for the x-, y-, and z-axis, respectively. It is possible to represent the attitude by another set of parameters known as quaternions. This representation is more robust because it doesn't produce an error when the pitch angle approaches ±90° (gimbal lock) [1]. For the scope of this work, however, it is more convenient to use Euler angles because attitude dynamics are simplified in order to have three independent one-axis control systems.

The methodology described in this work is exemplified using Guatemala's first CubeSat mission as a case study. This CubeSat is intended to be deployed from the International Space Station (ISS) and is designed to conduct remote sensing – water color (contamination) monitoring, specifically. For these reasons, an ISS orbit is assumed and the proper operation of the ADCS is of paramount importance. This work's main objective is the design and modeling of a feedback controller for this CubeSat's ADCS, as well as to define the control requirements, the modeling and simulation of disturbance torques, and the optimization of the control system's response.

II. Disturbance Modeling

The sizing of actuators is based on two aspects of the mission: the nature and magnitude of the disturbance torques and the requirements imposed by the payload. To analyze the disturbance torques it is necessary to use a disturbance model that estimates their magnitude throughout an orbit.

A. Simulation Inputs

A computer script based on the CubeSat Toolbox API was used to compute

the disturbance torques acting on a 1U CubeSat due to atmospheric drag, magnetic dipole moment, gravity gradient and solar pressure. This script uses the Jacchia 1970 Atmosphere Model for the atmospheric drag. The magnetic drag calculation is based on a tilted dipole model from [2] using the 1995 International Geomagnetic Reference Field coefficients (IGRF1995). Also, the sun vector used for the solar pressure is calculated using data from the 1993 edition of the U.S. Government's Astronomical Almanac. The input parameters for the script were chosen in order to simulate a worst-case scenario for the disturbance torques acting on the CubeSat. Table 1 lists the CubeSat's mechanical parameters used in order to simulate the worst possible case within constraints imposed by CalPoly's 13th revision of the CubeSat Design Specification (CDS) [3]. A residual dipole moment of 1 A-m2 for each axis was assumed, based on the estimation that magnetic torques are the dominant source of disturbances as described in [4]. Another assumption made was that the CubeSat will maintain a constant attitude profile with respect to the Local Vertical Local Horizontal (LVLH) frame of reference. The center of gravity (C.G.) offset was chosen to be the maximum allowed by the CDS's requirements (2 cm from the geometrical center), and the mass was assumed to be uniformly distributed throughout the CubeSat volume. Finally, the CubeSat surfaces were modeled as solar panels in all the side faces, and as aluminum plates on the top and bottom faces.

Parameter	Value
CubeSat Type	1U
CubeSat Mass	1.33 kg
Surface Area	0.01 m^2
C.G Offset	<0.02,0.02,0.02> m
Dipole Moment	<0.01,0.01,0.01> $A \cdot m^2$ [4]
Inertia (I_{xx}, I_{yy}, I_{zz})	2.22×10^{-3} $kg \cdot m^2$
Earths Angular Velocity	7.291×10^{-5} rad/s
Drag Coefficient	2.2 [5]

Table 1.CubeSat parameters used for disturbance modeling. C.G. = center of gravity.

Because many CubeSats are now being deployed from the International Space Station (ISS), the orbital elements for the simulation were chosen to be that of the ISS (see Table 2). The altitude included in Table 2 is calculated by subtracting the earth´s mean radius [6] from the orbit´s semi-major axis.

Parameter	Value
Semi-major axis	6788.72 km (417.72 km altitude)
Inclination	51.64°
Right Ascension of the Ascending Node	101.33°
Argument of perigee	20.20°
Eccentricity	6.177×10^{-4}
Mean Anomaly	339.94°
Earths Angular Velocity	7.291×10^{-5} rad/s
Start Date (Julian)	April 1, 2014 (2.4567485×10^{6})
Duration	24 h

Table 2. Orbital elements used for disturbance simulation.

The start date for the disturbance simulation was chosen based on the maximum solar activity for sunspot cycle 24, which reached a peak in April 2014 [7]. The simulation was carried out for a 24-hour time span starting from the Julian Date that corresponds to the date of the solar peak. A 24-hour simulation corresponds to 15.521 orbit revolutions, where each orbit has a duration of approximately 92.78 min.

B. Simulation Outputs

The disturbance simulation model calculates the disturbance torques due to atmospheric, magnetic, gravitational and solar pressure. These calculations are conducted for the x-, y- and z-axes with respect to the CubeSat's body and the Earth Centered Inertial (ECI) frame of reference. The model used for the earth's magnetic field acts the strongest on the CubeSat's z-axis (Fig 1).

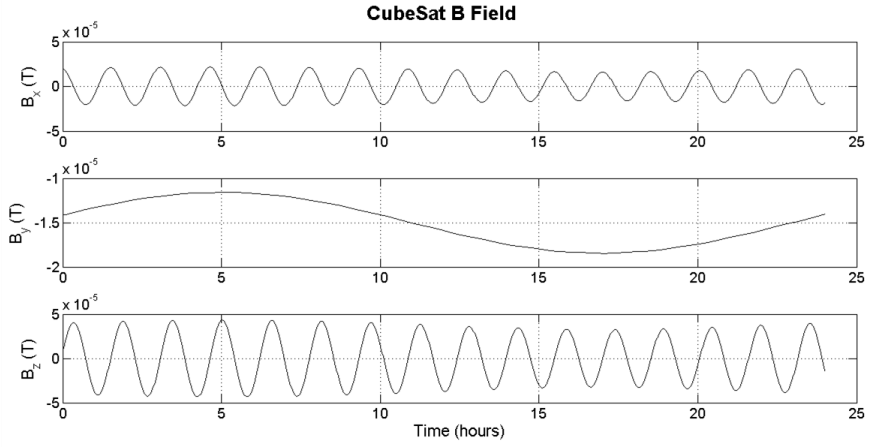

Fig. 1. Magnetic field acting on a CubeSat with the orbital elements of Table.

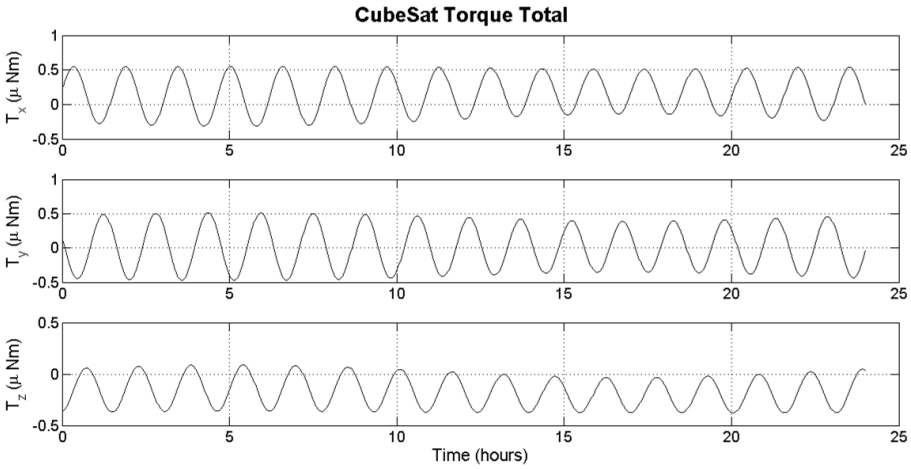

Fig. 2. Total torques acting on a CubeSat with an orbit similar to the ISS for a 24-hour time span.

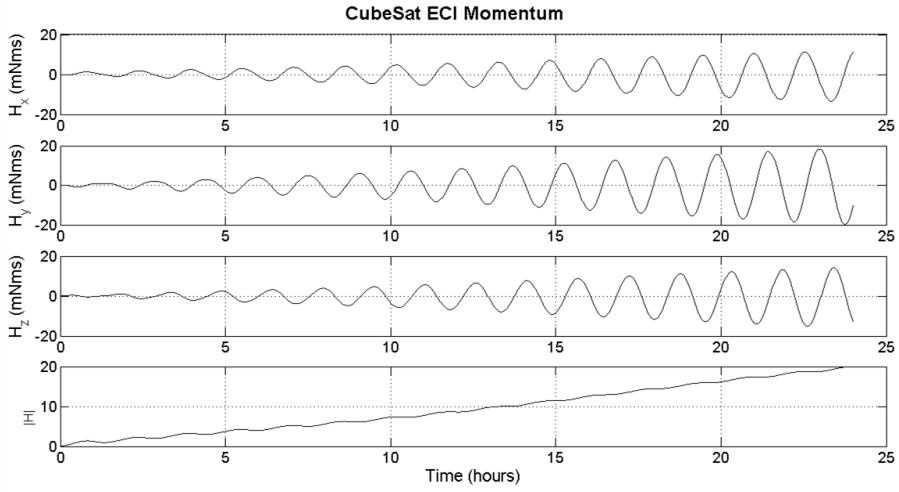

Fig. 3. Moment of a 1U CubeSat for an orbit similar to the ISS for a 24 hour time span.

III. Hardware Design

The selected control method follows a Zero Momentum control scheme using three reaction wheels as actuators. Table 3 summarizes the parameters that characterize the actuators needed to reject the expected disturbance torques. Based on the parameters derived from disturbance rejection requirements, it is possible to select a DC motor to be used as part of the reaction wheel assembly.

Actuator	Parameter	Result	Result*Safety Factor
Reaction Wheels	Maximum Torque	5.654×10^{-7} N·m	5.654×10^{-6} N·m
	Maximum Momentum	8.387×10^{-4} Nm·s	8.387×10^{-3} Nm·s
Magnetorquer	Dipole Moment	1.118×10^{-2} A·m^2	1.118×10^{-1} A·m^2

Table 3. Actuator sizing design parameters. The right-most column indicates the value when multiplied by a Safety Factor of 10.

Once the performance characteristics of the motor are defined, it is also possible to select the proper geometry and size for the flywheel (See Table 4). More details on the hardware design are being published separately.

Reaction Wheel Design	
Moment of Inertia	5.73×10^{-6} kg·m^2
Stored Momentum	8.82×10^{-3} Nm·s
Sat Time	1559.82 s
Flywheel Volume	3.32 cm^3
Flywheel Mass	29.13 g
Moment/Mass Ratio	1.97

Table 4. Design results for the reaction wheels.

V. Control System Model

The dynamics of a satellite can be approximated by the following set of equations:

$$T_{dx} + T_{cx} = I_x \ddot{\phi} \quad [1]$$

$$T_{dy} + T_{cy} = I_y \ddot{\theta} \quad [2]$$

$$T_{dz} + T_{cz} = I_z \ddot{\psi} \quad [3]$$

Here T corresponds to torque, the suffix d to external disturbance torques acting on the CubeSat, and c to the control torques generated by the reaction wheels, in the x-, y-, and z-axes (x, y, and z subindices, respectively). I is the CubeSat's inertia, where the suffix indicates the axis it is measured about.

When the CubeSat's body reference frame is placed so that its axes coincide with the structure's principal axes of inertia, the products of inertia in the satellite's inertia matrix are cancelled. The model consisting of eqs. [1], [2] and [3] makes the assumption that the system's inertia matrix is diagonal [8] by using the principal axes of inertia as the system's reference axes. From this assumption, the 3-axis attitude dynamics can be treated as three individual systems that control the attitude over each rotation axis independently.

A. ADCS Plant Representation

A plant is the mathematical model for the combination of a) the actuator and b) the process to be controlled. Typically, the relationship between the plant's input and its output is described using a transfer function in the frequency domain, which is a function of Laplace's variable, represented as s.

1. CubeSat Model

According to [9], the rotation of a satellite with respect to one axis can be modeled by a double integrator plant. By taking the Laplace transform of (1), (2) or (3), a transfer function that has torque as the input and the attitude as the output can be obtained:

$$\frac{\theta(s)}{T(s)} = \frac{1}{I \cdot s^2} \qquad [4]$$

In eq. [4] the constant I corresponds to the system inertia with respect to the rotation axis where the Euler angle is being measured.

2. Actuator Model

The torque input comes from the momentum exchange device. This device is known as a reaction wheel when it is used in the torque command mode. A simple model from [10] describes the reaction wheel dynamics as a torque actuator:

Notation	Description	Parameter
R	Terminal Resistance	22 Ohms
J	Rotor Inertia	0.69×10^{-7} kg·m^2
K_T	Torque Constant	3.64×10^{-3} Nm/A
K_V	Back-EMF Constant	0.38×10^{-3} V/rpm
B	Dynamic Friction Torque	2.60×10^{-9} Nm/rpm
I_W	Flywheel Inertia	5.73×10^{-6} kg·m^2
I_S	Satellite Inertia	8.00E-04 kg·m^2

Table 5. Values used to model the reaction wheel.

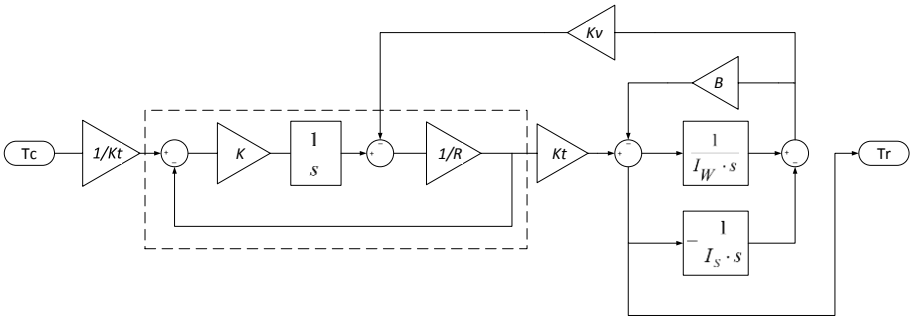

Fig. 4. Model of a momentum wheel in torque command mode.

The parameters used in this model (Fig.) correspond to the characteristics of the selected DC motor, the flywheel and an estimated inertia for the CubeSat (¡Error! No se encuentra el origen de la referencia.). *K* represents the forward gain inside the first loop, which is enclosed by the dashed line inside Fig. . This loop regulates the current, and allows the motor to be used as a torque actuator [10].

Because the dynamic friction torque *B* is several orders of magnitude smaller than the other variables in the model (see ¡Error! No se encuentra el origen de la referencia.), the effects of the dynamic friction torque can be neglected (B→0). And taking the fact that the satellite's inertia is several orders of magnitude greater than the flywheel's inertia ($I_S >> I_W$), the transfer function between the commanded torque (T_C) and the reaction torque (T_R) can be simplified as follows:

$$\frac{T_R}{T_c} = \frac{\frac{K}{s \cdot R}}{1+\frac{K}{s \cdot R}\left(1+\frac{K_V \cdot K_T}{K \cdot I_W}\right)} \qquad [5]$$

It is possible to simplify the transfer function even further by choosing a forward gain that satisfies the following relationship [11]:

$$K \gg \frac{K_V \cdot K_T}{I_W} \qquad [6]$$

By using the values from ¡Error! No se encuentra el origen de la referencia. it can be calculated that the value of *K* must be chosen to be greater than 2.42 in order to satisfy the condition of eq. [6]. This way the term inside the parenthesis in eq. [5] has an approximated value of 1, and the transfer function turns into that of a first-order system with a time constant depending only on the motor's terminal resistance, *R*, and the selected forward gain, *K*.

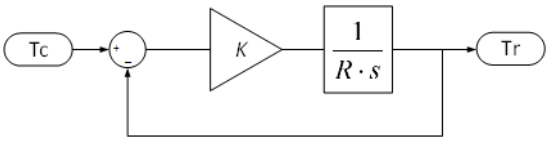

Fig. 5. Simplified model of the Reaction Wheel.

For this simplified model, it can be found that the transfer function between the command torque , T_C, and the reaction torque , T_R, is as follows [11]:

$$\frac{T_R}{T_C} = \frac{1}{1+s\cdot(R/K)} \qquad [7]$$

The selection of *K* has a direct effect on the system's response characteristics. The calculated value of 2.42 was used as an initial guesstimate for the value of *K*, and the design was further optimized using design optimization methods. The selected values for several figures of merit used as step response requirements are shown in Table 6.

Notation	Description	Parameter
T_R	Rise Time	$1.00\text{x}10^{-3}$ sec
T_S	Settling Time	$1.00\text{x}10^{-2}$ sec
P.O.	Percent Overshoot	2 %
P.U.	Percent Undershoot	1 %

Table 6. Parameters used as requirements for the selection of *K*.

From the optimization, the value for the forward gain that satisfies requirements was found to be of the order of 10^4. The new system step response can be seen in Fig. , which shows that it takes exactly 1 millisecond for the system to reach 80% of its final value. The stability of the system can be verified using a Nyquist Plot for the closed-loop from *Tc* to *Tr* (See Fig.). From the Simplified Nyquist criterion [12], it is known that the system can't become unstable because the closed contour for all possible frequencies does not encircle the critical point at $s = -1$, indicating that the reaction wheel simplified model is stable for any possible value of *K*.

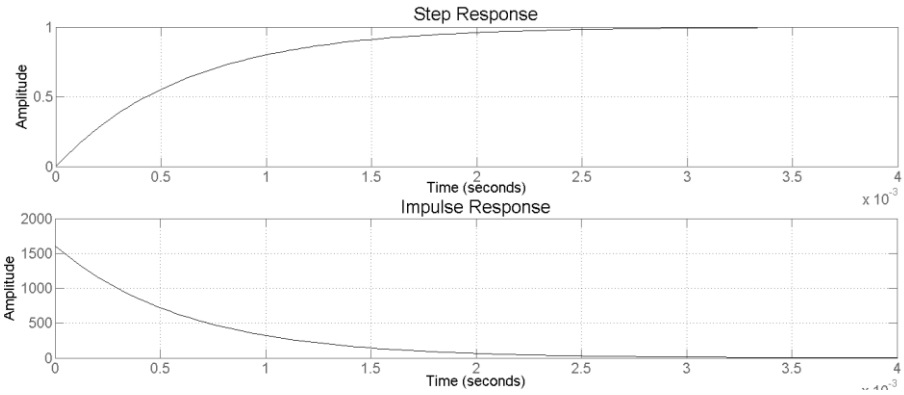

Fig. 6. Step and impulse response for the simplified reaction wheel model with a DC motor in a torque command configuration.

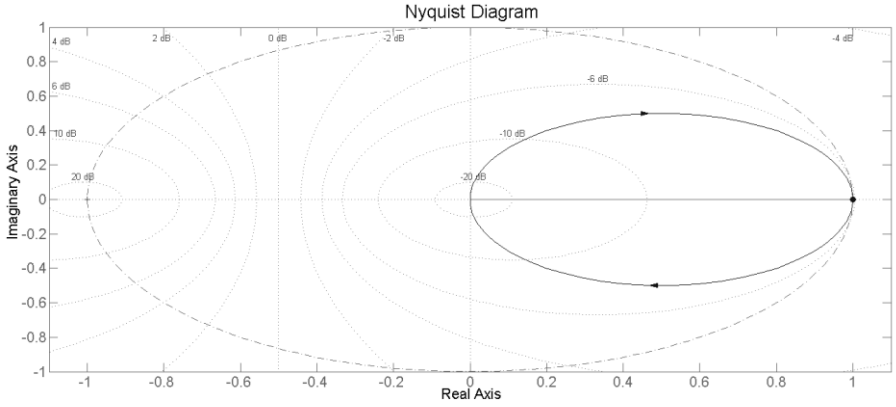

Fig. 7. Nyquist plot for the closed-loop reaction wheel model.

3. Complete Plant Representation

The total plant of the system is the combination of the actuator and the CubeSat attitude dynamics. The actuator and the CubeSat block are in series and therefore the transfer function of the whole plant can be obtained by multiplying eq. [4] by eq. [7]:

$$\frac{\theta(s)}{T_C(s)} = \frac{\frac{K}{R_M \cdot I_S}}{s^2\left(s+\frac{K}{R_M}\right)} \qquad [8]$$

The resulting plant in is a third-order system. The absolute stability of the control system can be verified by analyzing its open-loop response to different

input signals. From the open-loop impulse response plot (Fig.), it can be seen that the plant has an unbounded output. According to the definition of stability for a dynamic system [13], this type of response corresponds to an unstable system. This indicates that the controller to be designed has to stabilize the system while achieving the desired response characteristics. The following section addresses the design and validation of such a controller.

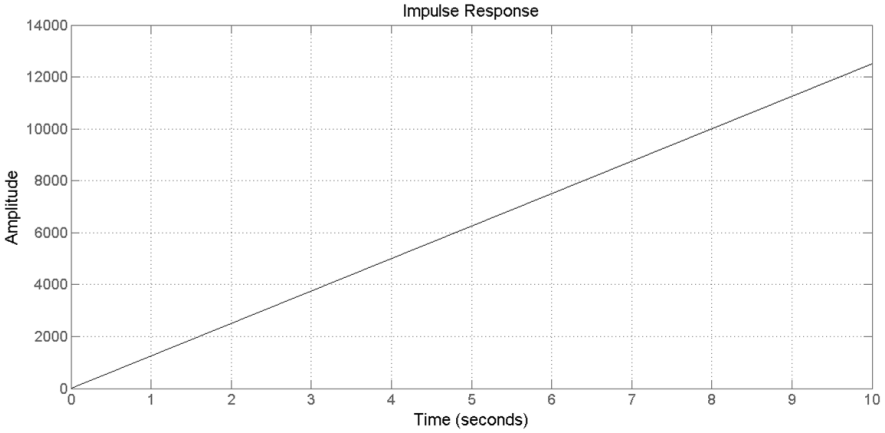

Fig. 8. Impulse response of the CubeSat Plant without the use of a closed-loop controller.

VI. ADCS Controller Design

A. Requirements:

As proposed in [14], the most basic attitude maneuver control loop for Euler angle error over one-axis is:

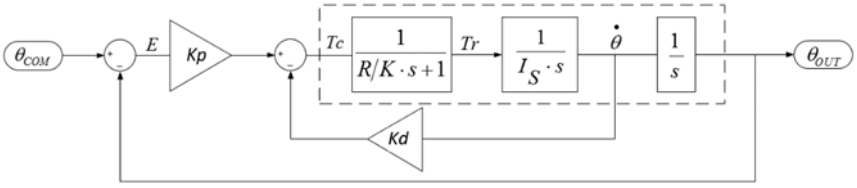

Fig. 9. Basic one-axis attitude control loop.

This design consist of an inner and an outer loop, both regulated proportionally. The inner loop is regulated by a factor *Kd* while the outer loop is by a factor of *Kp*. As outlined by the dashed section in

Fig. , the CubeSat's transfer function is divided in two different blocks. It is represented this way so that the angular rate can be measured by the inner

loop. By using block algebra, the feedback loop can be modified so that the plant is represented by one block. The blocks inside the dashed section in Fig. corresponds to the plant transfer function (see eq. [8]).

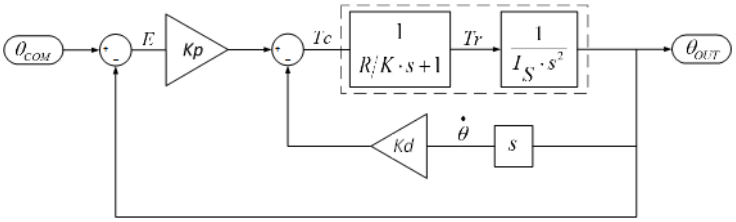

Fig. 10. Identification of the control system's plant.

This simplified model holds only when the following conditions are valid: a) the measurement noise in attitude and angular rate sensors is negligible, b) attitude commands are small ($\psi \approx 0, \theta \approx 0 \; and \; \varphi \approx 0$), c) there are negligible coulomb friction levels in the reaction wheel assembly (RWA), and d) the RWA doesn't reach its torque nor velocity saturation levels. As can be seen in Fig. 11, the use of unitary gains for the control loop configuration of

Fig. is enough to stabilize the CubeSat plant. Fig. shows the settling time required for the system to reach 2% of its final value. Other important characteristics of the system's initial transient response are shown in Table.

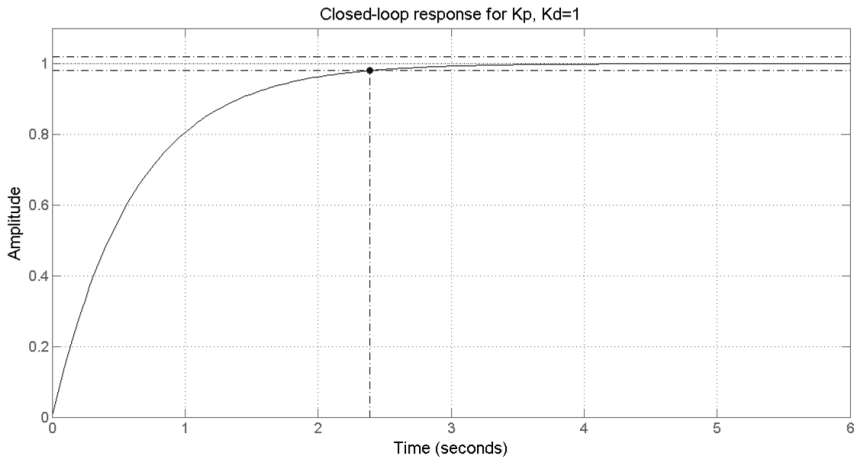

Fig. 11. Step response of CubeSat Plant using a system architecture for Euler angle and angular rate error correction with unitary controller gains.

B. Inner Loop Design

In the context of the CubeSat's ADCS, there are two major reasons to optimize the system's transient response. The first one is to make the system more robust in order to compensate for approximations and errors in the modeling

of the system components (actuators, dynamics, sensors, etc.). The second reason is to achieve a faster response [15]. The inner feedback loop is the part of the control system that generates damping. This inner feedback path acts on the derivative error of the system. This is critical because without this component, the system is inherently unstable. The root locus plot of the system without the derivative regulation demonstrates it would be unstable, because it contains poles that can only be in the right-half of the complex plane (Fig. 12).

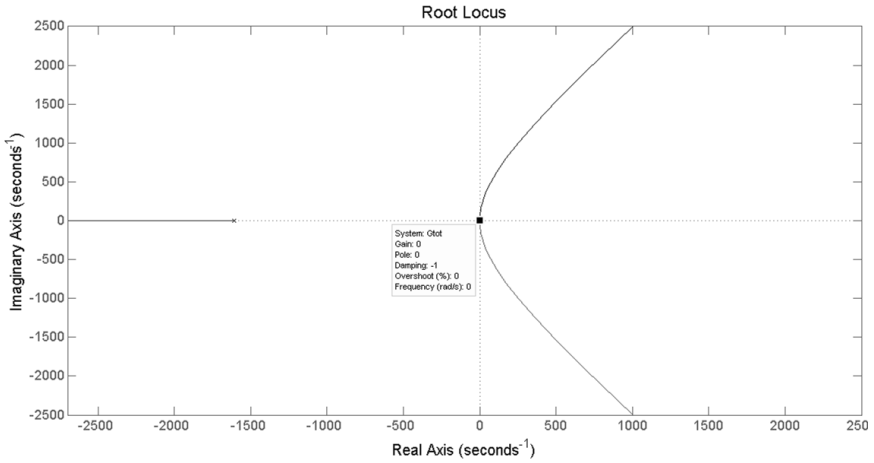

Fig. 12. Root locus plot of the system without derivative feedback show that its poles are located in the right-half of the complex plane.

The inner loop was first isolated in order to remove the effects of the outer loop [16]. Generally, a smooth non-oscillatory response is needed for the attitude control of satellites [17]. Therefore the system has to be overdamped, i.e. have a damping ratio (ζ) of at least 1. In order for the system to have low sensibility, the phase margin (P.M.) has to be restricted to an acceptable range (see eq. [10]). The performance optimization of the inner loop was based on the following control criteria:

$$\zeta \geq 1 \qquad [9]$$

$$180° > P.M. > 45° \qquad [10]$$

The controller gain K_d was optimized directly from the computer model using an initial guesstimate of 1. Several optimization methods were tested, but only one was able to yield a feasible solution for the given set of requirements. The pattern search method uses the “patternsearch” function in order to iteratively find a numerical solution to a minimization problem (see [18] for more information).

C. Outer Loop Design

The continuous controller design is going to be implemented on a micro-controller by means of emulation. Emulation is a method used to approximate a continuous controller design with a set of difference equations so that it can be implemented in discrete intervals established by a sample rate T_S. Therefore it is important to choose a system bandwidth that allows the computer to achieve a sample rate that is at least 30 times faster [19]. By anticipating a maximum sample period of 10 milliseconds (which is achievable by any of today's computers), the corresponding system bandwidth can be calculated in the following way:

$$\omega_b \cong \frac{1/T_S}{30} = 3.33Hz \cong 21\ {}^{rad}/_{S} \qquad [\ 11\ ]$$

By using block algebra in the control system of Fig. , it is possible to deduct the transfer function between the error signal E and the attitude command θ_{com}:

$$\frac{E(s)}{\theta_{com}(s)} = \frac{s^3\frac{R_m}{K}+s^2+s\frac{K_d}{I_S}}{s^3\frac{R_m}{K}+s^2+s\frac{K_d}{I_S}+\frac{K_p}{I_S}} \qquad [\ 12\ ]$$

Following the final value theorem one can use eq. [12] to calculate the steady-state error E_{SS} of the system for a given signal. This way it is possible to determine that for a unit-step input, the steady-state error will not be null:

$$E_{ss} = \lim_{s\to 0} s \cdot E(s) = \frac{I_s}{K_p} \qquad [\ 13\ ]$$

As demonstrated in eq. [13] the steady-state error has a finite value. For this reason it is necessary to incorporate an integral component as part of the outer loop. An additional integrator multiplies the denominator of eq. [12] by another *s* term. After this, the result became null when computing eq. [13] for a unit-step input. The outer-loop controller was ultimately designed using a computer based Proportional-Integral-Derivative (PID) tuning method. This method allowed the proportional and integral gains of the controller to be tuned based on the specified bandwidth and phase margin. A bandwidth of 21 rad/s and phase margin for the PI tuning process of 60° were selected from eq. 9 and 10, respectively.

D. Control Design Results

The final control system incorporates two feedback loops. The inner loop is regulated by a derivative controller, and the outer loop by a proportional-integral controller. This is commonly known as a PID regulated control system, where the integrator and derivation parts are operating in parallel. The results

of the optimization process for the different controller gains in each loop are presented in Table.

Controller	Parameter	Notation	Value
Inner Loop	Derivative Term	K_D	0.61129
Outer Loop	Proportional Term	K_P	12.64
	Integral Term	K_I	160

Table 7. Controller optimization results for one-axis control loop.

The performance of the general closed-loop system was improved significantly by optimizing the controller's design. The reduction in the settling time is of particular importance. The initial system with unitary proportional gains showed to be very slow compared to the final design. This can be appreciated by comparing the time scale of Fig. 11 against Fig. 13. The settling time was improved by 92%, but at the expense of adding overshoot to the system. The gain and phase margins were also reduced significantly, but are still within an acceptable range. As can be seen in Table, the system bandwidth was also increased and ended up being closer to the desired value calculated in eq. [11].

Notation	Description	*Kp, Kd* =1	Final Design
T_R	Rise Time	2.195 sec	0.0525 sec
T_S	Settling Time	3.909 sec	0.2925 sec
P.O.	Percent Overshoot	0.00 %	23.98 %
ω_b	Bandwidth	0.998 rad/s	32.71 rad/s
G.M.	Gain Margin	1.608×10^3 dB	75.55 dB
P.M	Phase Margin	180°	120°

Table 8. Improvement of transient response characteristics.

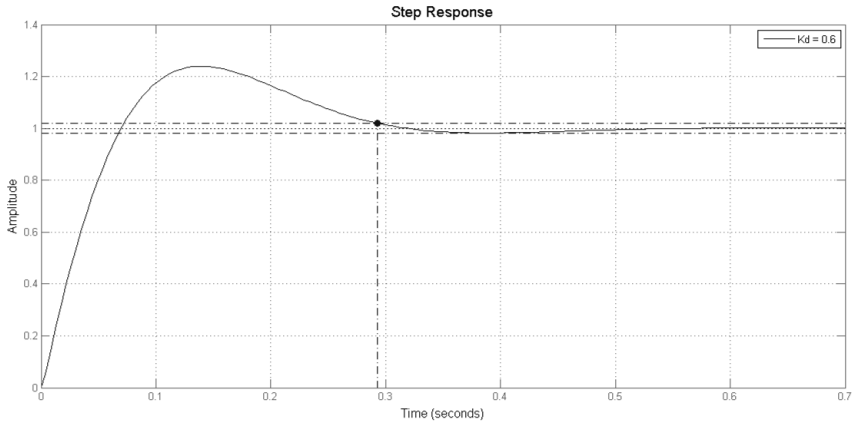

Fig. 13. System step response with PID controller.

E. Digital Implementation

A discrete computer model was created with a *z*-domain equivalent transfer function for the Proportional-Integral (PI) controller and the plant. Tustin's Approximation [20] was used to calculate the transfer function of the controller and a First-Order Hold equivalent was used for the plant. The resulting discrete system is shown in Fig. . By using this simulation model it was possible to check the effects of sample rates on the discrete approximation's performance. It was determined that a sample rate of 1000 Hz results in a discrete system that behaves almost the same as the continuous system (see Fig.). To illustrate the feasibility of achieving such a conversion rate, the K20 microcontroller family (Freescale, Tempe, AZ, USA) was taken as an example. The maximum achievable A/D conversion time of these microcontrollers is less than 2µs [21]. This corresponds to a conversion rate of 500 kHz, which is exactly 500 times faster than the required sample rate.

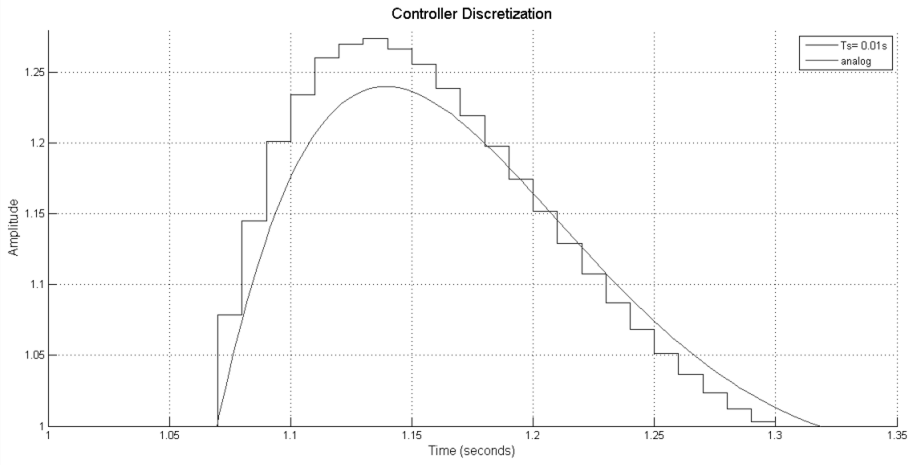

Fig. 14. Continuous vs. digital step response for a 100 Hz sample rate.

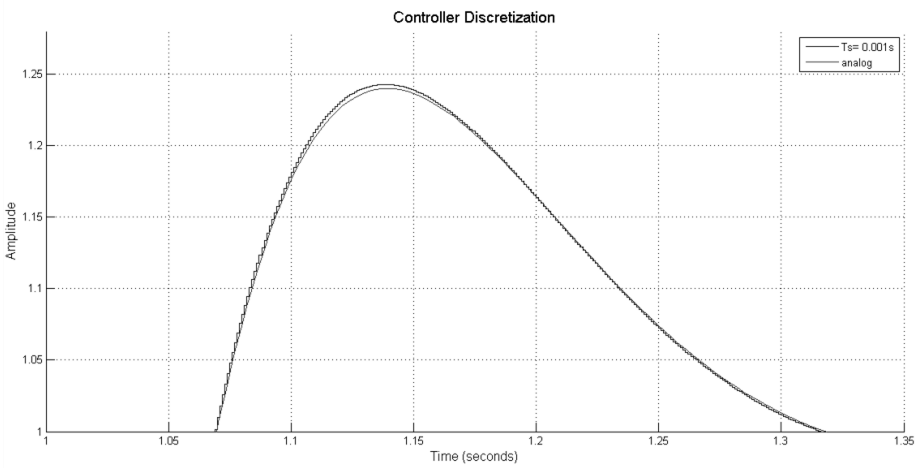

Fig. 15. Continuous vs. digital step response for a 1000 Hz sample rate.

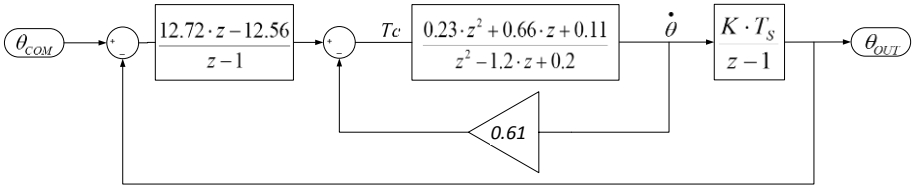

Fig. 16. Discrete approximation of the continuous control loop.

The continuous controllers designed in the previous sections can be implemented on a digital computer by using a set of difference equations. As shown in Fig. , the torque command sent to the plant results from the following operation:

$$T(z) = U(z) - Y(z) \qquad [14]$$

The difference equations relating the input and output of the controllers in each feedback loop can be derived using their respective transfer functions. The output of both controllers in the time domain can then be found to be:

$$\boldsymbol{u}(n) = u(n-1) + 12.72 \cdot e(n) - 12.56 \cdot e(n-1) \qquad [15]$$

$$y(n) = 0.6112 \cdot \dot{\theta}(n) \qquad [16]$$

Where *n* corresponds to the sample number taken exactly at each multiple of the sample period ($n=k \cdot T_S$). Finally, the control law used to regulate an attitude control loop for Euler angle correction using torque commands is:

$$t(n) = u(n) - y(n) \qquad [17]$$

With the control law consisting of eq. [15] and eq. [16], the continuous controller for the one-axis attitude control loop of

Fig. can be implemented in discrete intervals. These final set of equations are the outcome of the first iteration in the design of a controller for one-axis attitude control. This controller can be implemented by executing the arithmetic operations of eq. [17] with the attitude and rate error samples, and outputting the result as the torque command to the reaction wheel. This process is completed in-between samples, so that the output is updated before the next sample is taken. This way, the error is reduced continuously until the commanded attitude is the same as the sampled attitude (i.e. the system reaches stability). The before mentioned cycle is carried out each time the CubeSat's attitude has to be compensated as a result of an attitude step command or the attitude changes caused by environmental disturbance torques.

Conclusions

The greatest disturbance torque on a CubeSat results from the interaction between its dipole moment and the earth's magnetic field. When using the ISS's orbital parameters, this disturbance torque has its greatest effect on the CubeSat's yaw rotation angle. The ADCS's reaction wheel assembly will eventually saturate due to the increase of the total momentum norm, which is caused by constant disturbance torques. Every 24 hours the CubeSat will accumulate a total of 0.02×10^{-3} Nm·s. Thus, it is necessary to incorporate a momentum dumping mechanism to the designed attitude control loop. A reaction wheel with a DC motor, and a Flywheel designed to have an inertia of 5.73×10^{-6} kg·m^2 can be used as a torque actuator in order to reject the worst-case disturbance torque of 5.654×10^{-7} N·m. It was concluded that the characteristics of the selected DC motor and the system's inertia allow the reaction wheel model to be simplified into a first-order system with a time constant depending only on the motor's terminal resistance and the forward gain used in the reaction wheel's torque control loop. The model derived for the CubeSat plant corresponds to a system that has an unstable open-loop response. The simulation model showed that a double-loop configuration with one feedback path for angular rate error and another path for Euler angle error is enough to stabilize the system. Finally, it was concluded that the continuous controllers designed to compensate the closed-loop performance of one-axis attitude control system can be successfully emulated in a digital computer as long as the sample period of the A/D converter is smaller than 1 milliseconds.

Discussion

The first steps of the control system design process for a CubeSat's ADCS have been analyzed in this paper. Guatemala´s first CubeSat mission was used as a case study for the design process, which includes the selection of an adequate control method, the creation of a disturbance model, the definition of control-derived requirements, the sizing of the control actuators, and the design of a closed-loop controller for one-dimensional attitude corrections.

The disturbance model was the basis for the definition of the control-derived requirements. The different disturbance sources acting on the CubeSat include the atmospheric drag, solar pressure and magnetic dipole moment. The orbital parameters of the ISS were chosen because lately, more CubeSats are being deployed into orbit from the ISS, and so the results obtained from this disturbance simulation can be of higher value for future CubeSat missions. Results show the cyclic nature of the disturbance torques acting on the CubeSat. The disturbance caused by gravity gradient is practically zero because a constant attitude profile was assumed. When comparing the amplitude of the signals it can be seen that the greatest disturbance torques result from the interaction between the CubeSat's residual dipole moment and the earth's magnetic field. The total torque acting on the CubeSat is the most important one to consider for actuator sizing. This is the sum of all the disturbance torques and has a maximum value of 5.654×10^{-7} N·m in the *y*-axis (Fig. 2).

Another important result coming out of the disturbance simulation is the fact that the CubeSat's momentum grows over time. This can be seen in the magnitude of the total momentum in respect to the ECI frame, where the value of the norm tends to increase (Fig. 3). This indicates that the set of reaction wheels will eventually saturate do to the constant increase in the stored momentum. The saturation has to be counteracted by a second set of actuators that introduce an external force to the system, such as thrusters, magnetorquers, space tethers, etc.

Based on the performance parameters of the selected brushless direct current (BLDC) motor, a Flywheel that meets the inertia and momentum storage requirements was designed. Afterwards it was possible to model and analyze the theoretical performance of this reaction wheel assembly for its use in a torque command configuration. A simulation model for the reaction wheel was created in order to analyze the system's response, and to select a closed-loop proportional controller gain. Given that the reaction wheel's role in the general control system is to transduce a torque command into an actual torque to the system, it is crucial that it does so as fast as possible. The time it takes for the reaction wheel to deliver a torque limits the overall performance of the ADCS. For this reason the selection of the forward gain was based on requirements that are bound to the system's step response.

The last step carried out was the design of a digital controller for one-axis

attitude control. It is important to mention that attitude dynamics were simplified in order for the rotation angles to be controlled independently of each other. In this manner, the problem is reduced to the development of a single-input single-output control system designed to have the desired response characteristics and that can be replicated for the roll, pitch and yaw rotations. Another simulation model for the entire attitude control system was created, from which it was possible to see that the system is inherently unstable and there is a need to design a controller not only to improve the system's response characteristics, but also to stabilize it.

Finally, a double-loop control architecture was tested using the simulation model. By means of simulation it was possible to determine appropriate continuous controller gains for the inner and outer controller. The inner loop operates on the derivative error, and the outer loop and the Proportional-Integral (PI) error. In the end it was observed that the designed controller operates as a PID controlled system. In order for the design results to be of use, the continuous design was approximated as a discrete system.

A very important aspect to consider when emulating a continuous controller is the sample rate of the analog to digital (A/D) converter. If the sample rate is chosen to be too small then the response has a tendency to increase in overshoot and degrade in damping [19]. This tendency can be seen in Fig. 14, where the controller was emulated using a sample period of 10 milliseconds. In this figure, it is shown that a 100 Hz sample rate is not enough for the discrete controller to accurately emulate the overshoot and damping characteristics of the continuous controller. With these results, it is possible to further simulate the attitude control system for Euler angle corrections over the CubeSat's three axes of rotation. The control of each rotation can be achieved with three independent attitude control loops, each incorporating a digital controller that is programmed to calculate its output by implementing eq. [17].

The immediate next step in the design of the ADCS is to incorporate an additional actuator to the control loop that introduces an external torque to the system when the reaction wheel reaches saturation levels. As stated in section VI, the designed attitude control system is limited to small attitude adjustments, or operations where a constant attitude profile needs to be maintained. For larger slew maneuvers, it is necessary to use a time optimal control strategy such as a bang-bang controller. Future work will be focused in the creation of an algorithm that achieves an adequate transition between the operations mode for large slew maneuvers and finer attitude adjustments.

References

[1] CHRobotics, “Understanding Euler Angles,” no. 1.1, pp. 7–8, 2013.

[2] J. R. Wertz, “Magnetic Field Models,” in *Spacecraft Attitude Determination and Control*, Dordrecht: Kluwer Academic Publishers, 1978, pp. 782–785.

[3] A. Mehrparvar, “CubeSat Design Specification,” *The CubeSat Program*, 2014. [Online]. Available: http://w.cubesat.org/images/developers/cds_rev13_final2.pdf. [Accessed: 27-Dec-2015].

[4] S. Schalkowsky and M. Harris, “Spacecraft Magnetic Torquers,” *NASA Sp. Veh. Des. Criteria*, pp. 13–14, 1969.

[5] D. L. Oltrogge, A. Graphics, C. Springs, K. Leveque, and M. Park, “An Evaluation of CubeSat Orbital Decay,” *25th Annu. AIAA/USU Conf. Smallsats*, vol. II, no. 2, 2011.

[6] The Mathworks Inc., “Earth’s Radius,” 2015. [Online]. Available: http://www.mathworks.com/help/map/ref/earthradius.html. [Accessed: 15-Dec-2015].

[7] D. H. Hathaway, “Solar Cycle Predictions,” *NASA*. [Online]. Available: http://solarscience.msfc.nasa.gov/predict.shtml. [Accessed: 29-Dec-2015].

[8] M. J. Sidi, “Linearized Attitude Dynamics Equations of Motion,” in *Spacecraft Dynamics and Control*, New York: Cambridge University Press, 1997, pp. 110–111.

[9] M. Paluszek, P. Bhatta, P. Griesemer, J. Mueller, and S. Thomas, “Elementary Loop Compensation,” in *Spacecraft Attitude and Orbit Control*, vol. 1, Plainsboro: Princeton Satellite Systems Inc., 2012, pp. 175–177.

[10] M. Paluszek, P. Bhatta, P. Griesemer, J. Mueller, and S. Thomas, “Reaction Wheel Model,” in *Spacecraft Attitude and Orbit Control*, Plainsboro: Princeton Satellite Systems Inc., 2012, p. 103.

[11] M. Paluszek, P. Bhatta, P. Griesemer, J. Mueller, and S. Thomas, “Model of the Momentum Exchange Device,” in *Spacecraft Attitude and Orbit Control*, Plainsboro: Princeton Satellite Systems Inc., 2012, pp. 161–164.

[12] K. J. Astrom and R. M. Murray, “The Nyquist Criterion,” in *Feedback Systems*, v2.11b ed., Princeton: Princeton University Press, 2012, pp. 270–278.

[13] R. C. Dorf and R. H. Bishop, “The Concept of Stability,” in *Modern Control Systems*, Upper Saddle River: Prentice Hall, 2011, pp. 387–391.

[14] M. J. Sidi, “Basic Control Loop for Linear Attitude Maneuvers,” in *Spacecraft Dynamics and Control*, New York: Cambridge University Press, 1997, pp. 164–165.

[15] G. F. Franklin, J. D. Powell, and M. Workman, “Problem Definition,” in *Digital Control of Dynamic Systems*, 3rd ed., Menlo Park: Addison Wesley, 1998, pp. 1–5.

[16] The Mathworks Inc., “Multi-loop Compensator Design,” 2015. [Online]. Available: http://www.mathworks.com/help/control/getstart/multi-loop-compensator-design.html. [Accessed: 15-Dec-2015].

[17] M. Paluszek, P. Bhatta, P. Griesemer, J. Mueller, and S. Thomas, *Design the Control Algorithms*. Plainsboro: Princeton Satellite Systems Inc., 2012.

[18] The Mathworks Inc., “How the Optimization Algorithm Formulates Minimization Problems,” 2015. [Online]. Available: http://www.mathworks.com/help/sldo/ug/how-the-optimization-algorithm-formulates-minimization-problems.html. [Accessed: 14-Dec-2015].

[19] G. F. Franklin, J. D. Powell, and M. Workman, “Digitization,” in *Digital Control of*

Dynamic Systems, 3rd ed., Menlo Park: Addison Wesley, 1998, pp. 58–68.

[20] M. Paluszek, P. Bhatta, P. Griesemer, J. Mueller, and S. Thomas, "Transforming From the S Plane to the Z Plane," in *Spacecraft Attitude and Orbit Control*, Plainsboro: Princeton Satellite Systems Inc., 2012, pp. 185–188.

[21] Freescale Semiconductor, "Sample time and Total Conversion Time," in *K20 Sub-Family Reference Manual*, Tempe: Freescale Semiconductor Inc., 2012, p. 685.